Melting of Lithium Hydride under Pressure

Tadashi Ogitsu, Eric Schwegler, François Gygi, and Giulia Galli

Lawrence Livermore National Laboratory, P.O. Box 808, Livermore, California 94550, USA

(Received 4 June 2003; published 22 October 2003)

We have computed the melting line of lithium hydride up to 200 GPa using the two-phase simulation technique coupled with first-principles molecular dynamics. Our predicted melting temperature at high pressures varies slowly with compression, ranging from 2000 to 2450 K at 50–200 GPa pressures. The compressed fluid close to the melting line retains the ionic character of the low pressure molten state, while at higher temperatures dynamical hydrogen clustering processes are observed, which are accompanied by changes in the electronic structure.

DOI: 10.1103/PhysRevLett.91.175502 PACS numbers: 61.20.Ja, 62.50.+p, 71.15.Pd

Lithium hydride (LiH) is the simplest alkali hydride, possibly the simplest compound material, and its electronic and structural properties have been the subject of extensive investigation [1–5]. Recently, single crystal x-ray diffraction experiments under pressure have been carried out at room temperature for both LiH and LiD. These measurements indicated that LiH (LiD) is stable in the rocksalt structure up to 36 GPa (94 GPa) [4], while all other alkali hydrides are known to transform to a CsCl structure at lower pressures: 1.2, 2.2–3.1, 4.0, and 28.0–32.0 GPa for CsH, RbH, KH, and NaH, respectively [3,6]. However, despite the remarkable progress reported in the past decade by both the diamond anvil cell [7] and shock physics communities [8], experimental studies of compressed low-Z materials remain a challenging problem. To date, the high pressure, high temperature phase diagram of LiH is largely unknown.

Accurate first-principles methods can complement and help interpret high-pressure experiments: They can provide a detailed description of the structural and bonding changes that a material undergoes under extreme conditions, as well as accurate determinations of melting temperatures (T) as a function of pressure (P). However, given the high computational cost in determining phase boundaries, first-principles simulations have been used in only a few cases to compute melting temperatures. Specifically, first-principles free energy calculations using the potential switching method have been used to compute Si [9] and Al [10] melting temperatures, as well as the Fe [11] melting line at high pressure. Unfortunately, these calculations are very demanding and their efficiency depends on the existence of an accurate empirical potential for the specific system and thermodynamic conditions of interest.

Recently, a simple yet accurate method for the determination of melting temperatures has been proposed [12]. This technique, called the two-phase (or coexistence) simulation method, is based on the direct comparison of liquid and solid free energies by performing constant-pressure, constant-temperature molecular dynamic (MD) simulations of slabs containing the two phases separated by an interface. Until now, the two-phase simulation technique has been applied only in the context of MD simulations using empirical potentials.

In this Letter, we have coupled the two-phase simulation method with first-principles molecular dynamics, and we have carried out a study of the melting line of LiH under pressure. Our predicted melting temperatures vary slowly with compression at high pressures, ranging from 2000 to 2450 K in the 50–200 GPa pressure range. In addition, we have investigated the structural and bonding properties of the molten state. Our results show that the compressed fluid close to the melting line retains the ionic character of the low pressure molten state. At higher T, dynamical hydrogen clustering processes are observed, which are accompanied by significant changes in the electronic structure properties.

We performed first-principles simulations using the Car-Parrinello (CP) method [13] and we treated the Li and H nuclei as classical particles. Although quantum effects are important to accurately determine the properties of LiH at zero T, e.g., its equilibrium lattice constant, melting temperatures (T_m) and equation of state data at high T are affected only weakly by quantum effects [14]. For example, the difference between the LiH and LiD melting temperatures at ambient P is only 2 K. The electron-electron and electron-ion interactions were described within density functional theory, with the Perdew-Burke-Ernzerhof generalized gradient approximation (GGA) [15] for the exchange-correlation energy and potential. A plane-wave basis set and Troullier-Martins pseudopotentials [16] were used with a maximum kinetic energy cutoff of 40 Ry [17]. The simulation cells consisted of 432 atoms (216 atoms in the liquid layer and 216 atoms in the solid layer), and the Γ point was used only to sample the supercell Brillouin zone. Finite size effects on the lattice constant of the solid are 1% when using 216 atom cells and the Γ point, as compared to a fully converged k-point calculation (4096 k points with eight atoms per cell).

In our two-phase simulations, the initial configurations of the solid and liquid phases were generated by single phase constant-volume MD runs; configurations obtained in this manner were then combined in a single supercell

with a small vacuum area between the solid and the liquid layer. The solid and the liquid phases were heated independently to reduce the strain near the interface. We performed two-phase simulations of LiH at 0, 20, 100, 150, and 200 GPa [18]. In order to assess whether configurations originally prepared in a liquid or solid state would solidify or melt, the mean square displacements of atoms, variations in equilibrium volumes, and changes in pair correlation functions were monitored as a function of the simulation time. For example, in Fig. 1 the discontinuity in the average volume observed between 2200 and 2300 K at 100 GPa is shown, which is indicative of melting. Calculations of the pair distribution functions [$g(r)$] and atomic mean square displacements under conditions close to the observed discontinuity confirmed that the samples below and above the discontinuity were indeed in the solid and liquid phases, respectively (see the inset of Fig. 1).

The melting temperature of LiH as a function of pressure predicted by our simulations is shown in Fig. 2. Experimentally, T_m of LiH has been determined only at ambient pressure. Our computed value at $P = 0$, $T_m^{0\ \mathrm{GPa}} = 790 \pm 25$ K, is about 18% lower than the experimental value, $T_m^{\mathrm{exp}} = 965 \pm 2$ K [20]. The most likely sources of error are due to the GGA [10] and possibly to inaccuracies introduced by the CP method, where the electrons are close to, but not exactly on, the Born-Oppenheimer (BO) surface. We have calculated the difference ($\Delta P_{\mathrm{CP\text{-}BO}}$) between the pressure obtained within CP-MD and BO-MD above and below the computed melting temperatures at the macroscopic densities determined by CP-MD. The values of $\Delta P_{\mathrm{CP\text{-}BO}}$ at 0, 20, 100, 150, and 200 GPa are -0.28 ± 0.03, -0.29 ± 0.03, -2.33 ± 0.11, -2.62 ± 0.19, and -4.01 ± 0.17 GPa, respectively. Therefore, CP dynamics leads to a few percent underestimation of T_m at all pressures; we estimate that the error in T_m at low P is approximately 5% due to inaccuracies introduced by CP dynamics, and the remainder due to the GGA. It is interesting to note that all of the melting temperatures calculated within local density approximation (LDA) or GGA reported in the literature underestimate the corresponding experimental values at low pressure [9–11], e.g., 16% in Al and 20% in Si. This effect may be due to the general tendency of the LDA to overestimate the stability of the liquid phase with respect to the solid state in cases where, upon melting, the electronic charge density tends to become more homogeneous.

As seen in Fig. 2, the melting curve is very steep below 20–30 GPa and becomes rather flat between 50 and 200 GPa. A similar behavior of T_m as a function of P has been observed for other ionic systems, e.g., LiF, NaCl, KBr, KCl, and CsI by Bohler *et al.* [21,22] using laser heated diamond-anvil cell experiments.

We now turn to the discussion of the structural and bonding properties of the liquid. The pair correlation functions at low and high pressures, at four different (P, T) conditions, are shown in Fig. 3; in all cases, correlation functions characteristic of a molten salt are observed. We find that the Li-H ionic bond is very stiff and its length depends weakly on pressure, as indicated by the position of the first peak of $g^{\mathrm{Li\text{-}H}}(r)$ which does not scale with the cubic root of the density, $a = \sqrt[3]{\rho}$. On the other hand, H-H and Li-Li distances do scale with a. The coordination numbers defined by the integration of $g^{ij}(r)$ up to the first minimum indicate that, while the coordination of H around Li does not change under pressure, i.e., it remains constant at about 6; the H-H and Li-Li coordinations increase from 12 at ambient P to about 20 at 100 GPa. An additional indication, that in spite of some structural changes in the second and third neighbor coordination shells the ionic character of the Li-H bond is retained in the high P fluid, comes from the computed diffusion coefficients of Li and H. The results obtained at 100 GPa, close to the melting temperature, are shown in Fig. 4. It is seen that Li and H diffusion coefficients are very similar, in spite of the ratio between their masses, m_{Li}:$m_{\mathrm{H}} \approx 1$:7, which is clearly reflected in their respective velocity

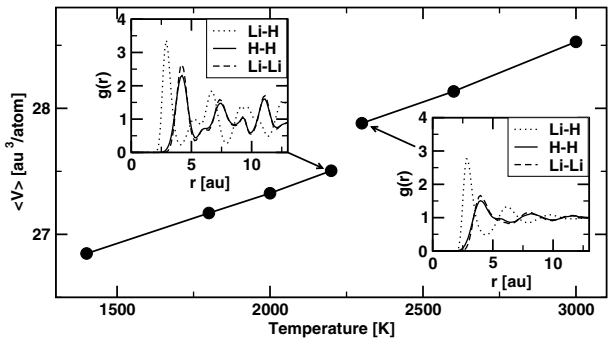

FIG. 1. Computed average volume as a function of temperature at 100 GPa. Solid circles represent data obtained in our simulations, and the lines are guides to the eye. The statistical error bars are smaller than the size of the circles. Insets: Pair correlation functions [$g(r)$] at 2200 K (left) and 2300 K (right) (see text).

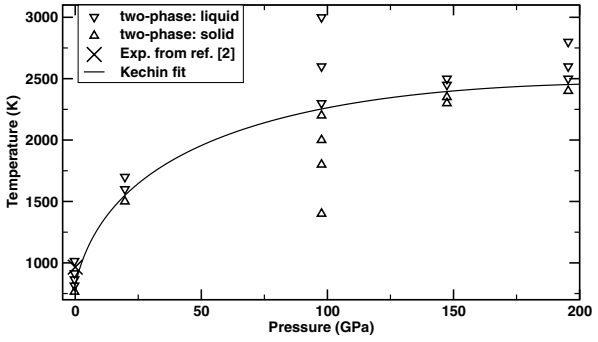

FIG. 2. The predicted melting line of LiH. Our calculated melting temperatures are: $T_m^{0\ \mathrm{GPa}} = 790 \pm 25$ K, $T_m^{20\ \mathrm{GPa}} = 1550 \pm 50$ K, $T_m^{100\ \mathrm{GPa}} = 2250 \pm 50$ K, $T_m^{150\ \mathrm{GPa}} = 2400 \pm 50$ K, $T_m^{200\ \mathrm{GPa}} = 2450 \pm 50$ K. These values include BO-MD corrections (see text) and the solid line is obtained using a Kechin fit [19] of the simulation data: $T_m(P) = 790[1 + 0.3911(P + 0.28)]^{0.3221} e^{-0.001373(P+0.28)}$.

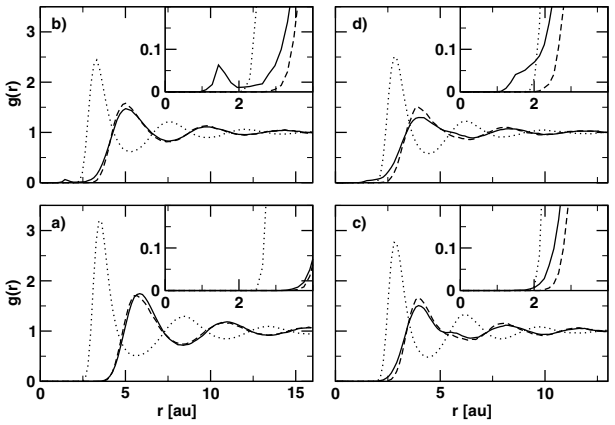

FIG. 3. The pair correlation functions of liquid LiH at (a) 1015 K and 0 GPa, (b) 2200 K and 12.9 ± 0.1 GPa, (c) 2300 K and 100 GPa, and (d) 3000 K and 100 GPa. H-H, solid line; Li-H, dotted line; Li-Li, dashed line. Inset: The region below 4 a.u. is enlarged to show the probability of hydrogen cluster formation.

distribution [see Fig. 4(b)]. The similarity in the Li and H diffusion coefficients indicates that the motion of neighboring lithium and hydrogen atoms is strongly correlated because of their ionic bond, and thus the two atomic species diffuse together for long periods of time. The fast motion of hydrogen atoms is mostly a vibrational and rotational/librational motion around a neighboring lithium atom and it does not contribute to the diffusion constant.

Close to the melting line, over the pressure range considered here, we have found that the structure of the fluid is characteristic of an ionic liquid. However, when the temperature is raised above melting, hydrogen cluster formation processes are observed, which perturbs the ionic character of the fluid. As shown in the insets of Figs. 3(b) and 3(d), $g^{\mathrm{H\text{-}H}}(r)$ has a small but finite distribution at $r = 1.4$ a.u., which corresponds to the equilibrium bond length of the H_2 molecule. We have carried out single-phase constant-volume MD runs using the density at 0 GPa and 0 K, and raised the temperature to 2200 K, where dynamical H_2 molecule formation and dissociation processes are observed. By quenching the system down to 1015 K and releasing the pressure to 0 GPa, we obtained a fluid with a small number of H_2 molecules. One of the H_2 molecules persisted over more than 10 ps of simulation. At

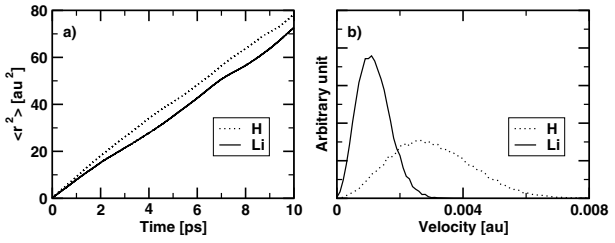

FIG. 4. (a) The mean square displacements of Li and H. (b) The velocity distributions of Li and H.

higher P and T (100 GPa, 3000 K), we also found dynamical clustering processes taking place. However, after quenching the system to 2300 K, no hydrogen clusters were found. This indicates that H_2 formation is likely to take place only at high T. It also suggests that the H_2 molecules observed at 0 GPa might depend on the initial configuration. A simulation at 0 GPa and 1015 K starting from a configuration at 2300 K and 100 GPa (where no hydrogen clusters are present) was then performed and no H_2 molecules were observed over 4 ps of simulation. In addition, we have computed the average energies of the samples at 0 GPa and 1015 K with and without H_2 molecules and found that the presence of H_2 molecules raises the total energy of the fluid by 3.0 ± 0.3 eV/cell, indicating that the H_2 molecules are most likely in a metastable state at ambient pressure and low T ($\simeq$1000 K).

The charge state of the H_2 molecule observed in the fluid raises simple yet fundamental questions. When the system is in an ionic configuration, Li atoms are positively charged and H atoms are negatively charged. If a pair of H atoms formed a molecule without changing the charge state of the original atoms, the antibonding level of the H_2 molecule would have to be occupied and the molecule would be unstable. Alternatively, if the excess electrons on H_2 are transferred to the bulk fluid, one may expect the overall ionicity of the liquid would be weakened, possibly causing the system to become less stable.

We have calculated the electronic structure of liquid LiH with and without H_2 at 0 GPa and 1015 K, and have analyzed the effect of H_2 molecule formation on the electronic structure. Approximately 50 atomic configurations were randomly selected from the MD runs, and the eigenstates calculated using the preconditioned steepest descent method combined with a subspace diagonalization scheme.

The calculated electronic density of states (EDOS) of the fluids with and without H_2 are shown in Fig. 5(a). In the EDOS without H_2, a clear energy gap between the valence and the conduction band is found, while in the EDOS with H_2 a pair of new levels appears below the valence band bottom (VBB) and above the valence band top (VBT). The level below the VBB is found to be a bonding state of the H_2 molecule, while the one above the VBT is a delocalized state. No eigenstates with an appreciable amplitude on the H_2 molecule have been found except for the H_2 bonding state, indicating that the charge state of the H_2 molecule is close to neutral. The electron released to the fluid upon formation of an H_2 molecule affects the overall ionicity of the liquid and it is responsible for a volume expansion. In our simulations, we observed $\langle V_{\mathrm{H_2}}^{0\ \mathrm{GPa}} \rangle = 94.06 \pm 0.26$ [a.u.^{3}/atom] and $\langle V_{\mathrm{No\ H_2}}^{0\ \mathrm{GPa}} \rangle = 93.37 \pm 0.10$ [a.u.^{3}/atom].

The EDOS at 100 GPa are shown in Fig. 5(b). At 2300 K, where H clustering does not take place, a clear energy gap is found and no states below the VBB are seen, while at 3000 K a significant amount of states below the VBB and around the Fermi level are observed. By

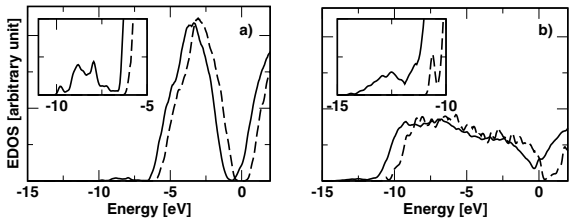

FIG. 5. Time averaged density of states, at (a) 0 GPa and 1015 K; solid (dashed) line denotes EDOS with (without) H_2 molecules. At (b) 100 GPa; solid (dashed) line denotes EDOS at 3000 K (2300 K). Inset: The region below the bulk valence band is enlarged to show the states associated with hydrogen cluster (molecule). The scales of the y axis are identical between (a) and (b).

inspecting the eigenstates, the levels below the VBB are identified as states related to H clusters, while those above the VBT are rather featureless. These levels are spread from the valence to the conduction band, without a clear gap [23].

In conclusion, we have coupled the two-phase simulation technique with first-principle molecular dynamics, and have computed the melting line and the structural and bonding properties of LiH under pressures up to 200 GPa. Our results show that, with moderate size supercells (432 atoms) and relatively short time scales ($\sim$5 ps), melting temperatures can be accurately computed as a function of compression from first principles. This opens the way to systematic studies of melting temperatures using density functional theory (DFT), for differently bonded systems, under various thermodynamic conditions. Our simulations show that, while LiH retains its ionic character in the liquid close to the melting curve, dynamical H clustering processes occur at higher T. We propose that the H clustering process could be evidenced experimentally by an increase of the liquid volume as a function of T, as well as by photoemission experiments, although this may be prohibitively difficult to carry out in a hot, compressed fluid. Finally, we note that, although the melting curves of alkali halides are located significantly higher in T than that of LiH, the behavior of the LiH melting line is similar to that of alkali halides, where a sharp rise in the low P regime is usually observed, followed by a flattening at high P.

The authors thank Professor Anatoly Belonoshko for stimulating discussions. This work was performed under the auspices of the U.S. Department of Energy at the University of California/ LLNL under Contract No. W-7405-Eng-48.

[1] E. E. Shpilrain, K. A. Yakimovich, M. E. Melnikova, and A. Y. Polishchuk, *Thermophysical Properties of Lithium Hydride, Deuteride, and Tritide and of Their Solutions with Lithium* (American Institute of Physics, New York, 1987).

[2] J. Hama, K. Suito, and N. Kawakami, Phys. Rev. B **39**, 3351 (1989).

[3] R. Ahuja, O. Eriksson, and B. Johanssen, Physica (Amsterdam) **265B**, 87 (1999).

[4] P. Loubeyre, R. L. Toullec, M. Hanfland, L. Ulivi, F. Datchi, and D. Hausermann, Phys. Rev. B **57**, 10 403 (1998).

[5] S. Lebègue, M. Alouani, B. Arnaud, and W. E. Pickett (to be published).

[6] H. D. Hochhemer, K. Strössner, W. Hönle, B. Baranowski, and F. Filipek, Z. Phys. Chem. Neue Folge **143**, 139 (1985); S. J. Duclos, Y. K. Vohra, A. L. Ruoff, S. Filipek, and B. Baranowski, Phys. Rev. B **36**, 7664 (1987).

[7] E. Gregoryanz, A. F. Goncharov, K. Matsuishi, H.-k. Mao, and R. J. Hemley, Phys. Rev. Lett. **90**, 175701 (2003); P. Loubeyre, F. Occelli, and R. LeToullec, Nature (London) **416**, 613 (2002); V. Iota and C.-S. Yoo, Phys. Rev. Lett. **86**, 5922 (2001).

[8] M. D. Knudson, D. L. Hanson, J. E. Bailey, C. A. Hall, and J. R. Asay, Phys. Rev. Lett. **90**, 035505 (2003).

[9] O. Sugino and R. Car, Phys. Rev. Lett. **74**, 1823 (1995).

[10] L. Vočadlo and D. Alfè, Phys. Rev. B **65**, 214105 (2002).

[11] D. Alfè, M. J. Gillan, and G. D. Price, Nature (London) **401**, 462 (1999); D. Alfè, G. D. Price, and M. J. Gillan, Phys. Rev. B **65**, 165118 (2002).

[12] J. Mei and J. W. Davenport, Phys. Rev. B **46**, 21 (1992); J. R. Morris, C. Z. Wang, K. M. Ho, and C. T. Chan, Phys. Rev. B **49**, 3109 (1994); A. Belonoshko, Geochim. Cosmochim. Acta **58**, 4039 (1994); O. Tomagnini, F. Ercolessi, S. Iarlori, F. D. D. Tolla, and E. Tosatti, Phys. Rev. Lett. **76**, 1118 (1996).

[13] R. Car and M. Parrinello, Phys. Rev. Lett. **55**, 2471 (1985).

[14] See, for example, pages 12, 55, and 56 of Ref. [1].

[15] J. P. Perdew, K. Burke, and M. Ernzerhof, Phys. Rev. Lett. **77**, 3865 (1996).

[16] N. Troullier and J. L. Martins, Phys. Rev. B **43**, 1993 (1991). Pseudopotentials with s-nonlocal, p-local, and s-local, p, d-nonlocal were used for H and Li, respectively.

[17] Constant resolution in the simulations was achieved with a 45 Ry cutoff energy combined with a three-dimensional well potential in momentum space with a 40 Ry radius to mimic the constant cutoff energy at 40 Ry.

[18] The total time simulated was $\sim$80 ps, which corresponds to a run time of $\sim$180 days on a 64-node Linux cluster of 1.5 GHz dual AMD processors and a Myrinet switch.

[19] Vladimir V. Kechin, Phys. Rev. B **65**, 052102 (2001).

[20] C. E. Messer and I. S. Levy, Inorg. Chem. **4**, 543 (1965).

[21] R. Boehler, M. Ross, and B. Boercker, Phys. Rev. B **53**, 556 (1996).

[22] R. Boehler, M. Ross, and D. B. Boercker, Phys. Rev. Lett. **78**, 4589 (1997).

[23] GGA (LDA) is known to underestimate the electronic band gap of semiconductors and insulators and thus only qualitative statements about the comparison between samples with and without hydrogen molecules are reported here. More quantitative studies of band gap closure in the liquid under pressure would require methods beyond the GGA of DFT.